AIAA JOURNAL
Vol. 38, No. 4, April 2000

Evolution of an Isolated Turbulent Trailing Vortex

Stefan Wallin*
Aeronautical Research Institute of Sweden (FFA), SE-161 11 Bromma, Sweden
and
Sharath S. Girimaji†
NASA Langley Research Center, Hampton, Virginia 23681

The long-time development of an isolated wing-tip turbulent vortex has been studied by Reynolds-averaged Navier–Stokes computations. The vortex is assumed to extend to infinity and to be axisymmetric and homogeneous in the axial direction, and the axial velocity is assumed to be negligible. The validity of different turbulence models, ranging from Reynolds stress transport models to eddy-viscosity K–ε models, has been assessed and qualitative comparisons with field measurements are made. Reynolds stress transport models correctly predict strong suppression of the turbulence in the rotation-dominated vortex core and a reasonable decay rate of the vortex. Outside of the core, the different Reynolds stress models differ significantly. The standard eddy-viscosity K–ε model is insensitive to rotation and, thus, overpredicts the vortex decay rate. Computations using explicit algebraic Reynolds stress models that are strictly based on Reynolds stress transport models show that the algebraic form compares reasonably well with the full transport form. It is, however, important that the curved flow algebraic assumption is invoked when deriving the explicit algebraic model.

Nomenclature

$\boldsymbol{a}$	= Reynolds stress anisotropy tensor, a_{ij}
B	= span width
$\mathcal{D}_{ij}$, $\mathcal{D}^{(K)}$, $\mathcal{D}^{(\varepsilon)}$, $\mathcal{D}^{(a)}_{ij}$	= molecular and turbulent diffusion of τ_{ij}, K, ε, and a_{ij}
e_{ij}	= dissipation rate anisotropy
II_S, II_{Ω^*}	= invariants of S_{ij} and Ω^*_{ij}
K	= turbulent kinetic energy
$\mathcal{P}_{ij}$, $\mathcal{P}$	= production of τ_{ij} and K
R_c	= core radius
r, θ, z	= radial, circumferential, and axial coordinates
$\hat{\boldsymbol{r}}$, $\hat{\boldsymbol{\theta}}$, $\hat{\boldsymbol{z}}$	= radial, circumferential, and axial unit vectors
$\boldsymbol{S}$	= mean flow strain rate tensor, S_{ij}
$\boldsymbol{T}$	= turbulent flux of Reynolds stresses, T_{ijk}
t	= time
$\boldsymbol{U}$	= mean velocity (r, θ, z), U_i
U, V, W	= mean velocity components (r, θ, z)
u, v, w	= fluctuating velocity components (r, θ, z)
Γ	= vortex circulation
ε	= dissipation rate of turbulent kinetic energy
ν	= molecular viscosity
Π_{ij}	= pressure–strain
$\bar{\bar{\tau}}$	= Reynolds stress tensor, τ_{ij} equal to $\overline{u_i u_j}$
$\boldsymbol{\Omega}$	= mean flow rotation rate tensor, Ω_{ij}
$\boldsymbol{\Omega}^*$	= modified mean flow rotation rate tensor, Ω^*_{ij}

Subscript

0	= initial

I. Introduction

THE long-time development of wing-tip vortices is of major interest in determining the safe distance between airplanes at takeoff and landing. The vortices persist for long times because the turbulence in the vortex core is strongly suppressed by the rotation. The vortex decays from the outer parts leaving the core more or less unaffected for long times, and thus, the radius of the maximum swirl velocity does not change much in time.

The decay mechanism for aircraft trailing vortices evolving in atmospheric turbulence is complex and involves several different processes. It is believed (Refs. 1–3 and others) that the decay mechanism is influenced by ambient atmospheric turbulence and stratification, three-dimensional vortex pair dynamic instabilities, and ground effects, as well as self-generated turbulence in the vortex. Each of these effects may be important at different conditions and should not be excluded in a complete analysis.

Coherent Doppler laser radar (LIDAR) measurements of trailing vortices of aircraft at takeoff and landing have been analyzed by Proctor,[1] and the overall conclusion is that there exist strong correlations between the vortex decay rates and ambient conditions. That suggests that the self-generated turbulence within the vortex is of secondary importance, especially during daytime when the atmospheric dissipation rates are high. The vortex dissipation mechanisms are complex, are not fully understood, and involve many different aspects that will not be addressed within this study. In a typical wake vortex, the Reynolds number is of the order of 10^7, which means that molecular diffusion is of lesser importance compared to turbulent diffusion.

Measurements of the near-field vortex rollup process[4,5] show that the vortex is initially fully turbulent. The source of turbulence is primarily the highly unstable shear layer from the wing trailing edge that winds up around the core. The winding of the vortex sheet generates a wakelike deficit in the axial velocity. That is another strong source of turbulence, shown by Ragab and Sreedhar[6] using large-eddy simulations. The turbulence in the vortex core is, however, strongly suppressed. It has been observed, experimentally as well as numerically, that the Reynolds shear stresses and turbulence production tend to zero approaching the vortex core. The reason for that is that the flow in the core is close to solid body rotation, which is strongly stabilizing. Because the Reynolds number is large, the core expands very little in time.

Farther downstream, the winding vortex sheet and the axial velocity deficit have been diffused by the turbulence, and any strong sources of turbulence do not exist any more. In this study, we will focus on this later stage of the vortex development. Because physical or numerical experimental data are rare for far-field vortices, we must rely on field observations and measurements. From field measurements the following features of trailing vortices have been

Received 24 March 1999; presented as Paper 99-3767 at the AIAA 30th Fluid Dynamics Conference, Norfolk, VA, 28 June–1 July 1999; revision received 1 September 1999; accepted for publication 2 September 1999.

*Research Scientist, Box 11021; Stefan.Wallin@ffa.se.
†Senior Staff Scientist, Institute for Computer Applications in Science and Engineering; currently Associate Professor, Aerospace Engineering Department, Texas A&M University, College Station, TX 77843.

established: 1) The core persists for a reasonable long period of time as the decay begins at the outer edges of the vortex and propagates inward. 2) There is no discernible overshoot in the circulation profile.

In a previous study by Zeman[7] of an isolated single vortex, it is reported that two-equation eddy-viscosity models, such as the $K-\varepsilon$ model, 1) strongly overpredict the decay rate of the vortex and 2) predict massive overshoots in circulation. The results obtained using a Reynolds stress transport (RST) model were in fact almost laminar. The turbulence shear stress $\overline{uv}$ was much lower than the molecular stress all over the vortex. The observed vortex decay is, however, much faster than laminar decay for the high-Reynolds-number vortices from a typical aircraft.

In an accompanying ongoing study by Wallin and Girimaji, single finite and infinite vortices using more advanced RST models are studied. Their results are more in line with observed trailing vortex behavior because they capture all of the qualitative aspects quite accurately. The objective of this study is to determine whether a two-equation explicit algebraic Reynolds stress model (EARSM) is indeed capable of capturing the observed features of the trailing vortex. This study is motivated by our ultimate goal of developing a three-dimensional unsteady Reynolds-averaged Navier–Stokes (RANS) capability for detailed investigation of trailing vortices. Clearly, for such an effort, a two-equation EARSM is more viable than the more expensive RST models.

We will later show the importance of the pressure–strain model in this highly rotating flow and that models based on the Speziale–Sarkar–Gatski (SSG)[8] model give results in line with observations whereas models based on the Launder–Reece–Rodi (LRR)[9] model give lower turbulence levels and, thus, a vortex decay rate slower than observed. This will explain the laminar solution that Zeman[7] obtained with the so-called isotropization of production model, which is close to the LRR model.

We will also show that explicit algebraic Reynolds stress models are capable of predicting the qualitative behavior if 1) the model is fully self-consistent, 2) the model is based on SSG, and 3) the weak equilibrium assumption is made in an appropriate curvilinear coordinate system.[10]

II. Modeling Assumptions

We will consider the wing-tip vortex in the farwake after any three-dimensional and time-dependent disturbances have vanished. The axial velocity component and the axial derivatives are assumed to be negligible. The vortex may, thus, be considered as axisymmetric, homogeneous in the axial direction, and developing in time.[11] It is, therefore, natural to express the flow in the vortex in a cylindrical coordinate system where $\hat{\boldsymbol{e}}_i = [\hat{\boldsymbol{r}}, \hat{\boldsymbol{\theta}}, \hat{\boldsymbol{z}}]$.

We define the spatial differentiation operator as

$$\nabla \equiv \hat{\boldsymbol{e}}_i \frac{\partial}{\partial x_i} \tag{1}$$

where

$$\frac{\partial}{\partial x_i} \equiv \left(\frac{\partial}{\partial r}, \frac{1}{r}\frac{\partial}{\partial \theta}, \frac{\partial}{\partial z}\right) \tag{2}$$

in a cylindrical coordinate system. In the problem considered, $\partial/\partial z \equiv 0$ because the axial direction is homogeneous. The problem is also homogeneous in the azimuthal direction, but the $\hat{\boldsymbol{\theta}}$ derivative may not be excluded from the nabla operator because the $\hat{\boldsymbol{\theta}}$ derivative of the unit vectors $\hat{\boldsymbol{r}}$ and $\hat{\boldsymbol{\theta}}$ are nonzero. Let us define the derivative of the unit vectors as follows:

$$\frac{\partial \hat{\boldsymbol{e}}_i}{\partial x_j} = \Gamma_{ijk}\hat{\boldsymbol{e}}_k \tag{3}$$

where Γ_{ijk} are all zero except $\Gamma_{122} = 1/r$ and $\Gamma_{221} = -1/r$. By the use of this definition, one may expand the gradient operating on any tensor of any rank simply by the use of the chain rule, that is, the gradient of the velocity expands to

$$\nabla \boldsymbol{U} = \hat{\boldsymbol{e}}_i \frac{\partial}{\partial x_i}(\hat{\boldsymbol{e}}_j U_j) = \hat{\boldsymbol{e}}_i \hat{\boldsymbol{e}}_j \left(\frac{\partial U_j}{\partial x_i} + \Gamma_{kij} U_k\right) \tag{4}$$

By the use of the preceding assumptions, the Reynolds-averaged velocity may be written as $\boldsymbol{U} = \hat{\boldsymbol{\theta}} V(r)$, and the Reynolds-averaged momentum equation in the $\hat{\boldsymbol{\theta}}$ direction reads

$$\frac{\partial V}{\partial t} = \frac{1}{r^2}\frac{\partial}{\partial r}\left(r^3 \nu \frac{\partial}{\partial r}\left(\frac{V}{r}\right) - r^2 \overline{uv}\right) \tag{5}$$

To close the momentum equation one needs an expression for $\overline{uv}$, which is the $\hat{\boldsymbol{r}}\hat{\boldsymbol{\theta}}$ component of the Reynolds stresses, $\bar{\bar{\tau}} = \hat{\boldsymbol{r}}\hat{\boldsymbol{r}}\overline{u^2} + \hat{\boldsymbol{\theta}}\hat{\boldsymbol{\theta}}\overline{v^2} + \hat{\boldsymbol{z}}\hat{\boldsymbol{z}}\overline{w^2} + (\hat{\boldsymbol{r}}\hat{\boldsymbol{\theta}} + \hat{\boldsymbol{\theta}}\hat{\boldsymbol{r}})\overline{uv}$.

A. Reynolds Stress Transport Modeling

Strong rotational and streamline curvature effects are present in the vortex. The stabilizing effects are in fact so strong that any preexisting turbulence in the core of the vortex is almost completely suppressed. It is, thus, believed that RST closures are needed to capture the turbulence physics properly. The transport equation for the Reynolds stress tensor in an inertial frame of reference may be written in symbolic form as

$$\frac{\mathrm{D}\tau_{ij}}{\mathrm{D}t} - \mathcal{D}_{ij} = \mathcal{P}_{ij} + \Pi_{ij} - \varepsilon\left(e_{ij} + \frac{2}{3}\delta_{ij}\right) \tag{6}$$

The molecular and turbulent diffusion $\mathcal{D}_{ij}$, the pressure-strain term Π_{ij}, and the dissipation rate anisotropy e_{ij} need to be modeled because they contain higher-order correlations. The production term is, however, explicit and reads

$$\mathcal{P}_{ij} = -(\tau_{ik}\boldsymbol{S}_{kj} + \boldsymbol{S}_{ik}\tau_{kj}) + (\tau_{ik}\boldsymbol{\Omega}_{kj} - \boldsymbol{\Omega}_{ik}\tau_{kj}) \tag{7}$$

where the mean flow strain and rotation rate tensors are

$$\boldsymbol{S} = \frac{1}{2}[(\nabla \boldsymbol{U})^T + \nabla \boldsymbol{U}] = \frac{1}{2}\left(\frac{\partial V}{\partial r} - \frac{V}{r}\right)(\hat{\boldsymbol{r}}\hat{\boldsymbol{\theta}} + \hat{\boldsymbol{\theta}}\hat{\boldsymbol{r}})$$

$$\boldsymbol{\Omega} = \frac{1}{2}[(\nabla \boldsymbol{U})^T - \nabla \boldsymbol{U}] = \frac{1}{2}\left(\frac{\partial V}{\partial r} + \frac{V}{r}\right)(\hat{\boldsymbol{\theta}}\hat{\boldsymbol{r}} - \hat{\boldsymbol{r}}\hat{\boldsymbol{\theta}}) \tag{8}$$

The standard form of the transport equation for the dissipation rate ε is adopted. For the vortex considered, the advection of ε, as well as the advection of any scalar quantity, is zero, and the equation for ε reads

$$\frac{\partial \varepsilon}{\partial t} - \mathcal{D}^{(\varepsilon)} = (C_{\varepsilon 1}\mathcal{P} - C_{\varepsilon 2}\varepsilon)\frac{\varepsilon}{K} \tag{9}$$

where the production $\mathcal{P} \equiv \mathcal{P}_{ii}/2$ and $\mathcal{D}^{(\varepsilon)}$ is the molecular and turbulent diffusion of ε. $C_{\varepsilon 1} = 1.45$ and $C_{\varepsilon 2} = 1.90$ is used.

The assumptions made for the vortex are that both the $\hat{\boldsymbol{z}}$ and $\hat{\boldsymbol{\theta}}$ directions are homogeneous. Moreover, the $\hat{\boldsymbol{r}}$ component of the mean velocity vanishes. The advection of the Reynolds stresses then only contain algebraic (nondifferential) terms that originate from the $\hat{\boldsymbol{\theta}}$ derivatives of the unit vectors. The material derivative in cylindrical coordinates, thus, becomes

$$\frac{\mathrm{D}\tau_{ij}}{\mathrm{D}t} = \frac{\partial \tau_{ij}}{\partial t} - \left(\tau_{ik}\Omega^{(r)}_{kj} - \Omega^{(r)}_{ik}\tau_{ki}\right) \tag{10}$$

where

$$\boldsymbol{\Omega}^{(r)} = (V/r)(\hat{\boldsymbol{\theta}}\hat{\boldsymbol{r}} - \hat{\boldsymbol{r}}\hat{\boldsymbol{\theta}}) \tag{11}$$

that is, the advection does not contain any spatial derivatives. With $V/r = \omega^R$, this term is actually half of the Coriolis term that appears in the Reynolds stress equation written in a rotating frame of reference, where ω^R is the (constant) rotation rate of the system. The other half of the Coriolis term originates from a similar transformation of the production term.

The modeling of the pressure–strain term is an important issue, especially in rotation-dominated flows. Models that are linear in the Reynolds stress anisotropy have been widely used due to the simplicity and general good behavior in a number of benchmark flows of engineering interest. Recently more attention has been placed on nonlinear models, for example, the SSG model,[8] which has been found to be superior to linear models in many aspects. In this study,

Table 1 Values of C coefficients for different linear pressure–strain models

Model	C_1^0	C_1^1	C_2	C_3	C_4
Linearized SSG	3.4	1.8	0.36	1.25	0.40
Original LRR	3.0	0	0.8	1.75	1.31
Recalibrated LRR	3.6	0	0.8	2	1.11

we will focus on the performance of EARSMs where only linear pressure–strain models may be considered.

The pressure–strain and dissipation rate anisotropy are usually lumped together into the general linear form (for example, see Ref. 12):

$$\begin{aligned}\Pi_{ij}/\varepsilon - e_{ij} &= -\tfrac{1}{2}\left[C_1^0 + C_1^1(\mathcal{P}/\varepsilon)\right]a_{ij} + C_2(K/\varepsilon)S_{ij} \\ &+ (C_3/2)(K/\varepsilon)\left(a_{ik}S_{kj} + S_{ik}a_{kj} - \tfrac{2}{3}a_{kl}S_{lk}\delta_{ij}\right) \\ &- (C_4/2)(K/\varepsilon)(a_{ik}\Omega_{kj} - \Omega_{ik}a_{kj})\end{aligned} \tag{12}$$

where the Reynolds stress anisotropy a_{ij} is defined as

$$a_{ij} \equiv \tau_{ij}/K - \tfrac{2}{3}\delta_{ij} \tag{13}$$

and $K \equiv \tau_{ii}/2$ is the turbulent kinetic energy. The classical LRR model[9] and the SSG model[8] linearized around equilibrium homogeneous shear may be included in this general form where the C coefficients are given in Table 1 (for example, see Ref. 13 for linearization of the SSG model).

The original calibration of the LRR model may not have been optimal in all situations, and more recent calibrations of the LRR model imply that the Rotta coefficient $c_1 \approx 1.8$ and the coefficient in the rapid pressure strain model $c_2 \approx 5/9$, for example, see Refs. 14–18. All LRR computations in this study were made using the recalibrated set of coefficients. The SSG model, also in the linearized form, is known to be superior to the LRR model in rotation-dominated flows, for example, Ref. 13, where the SSG model, the differential as well as its algebraic form, performs well for homogeneous rotating shear flows. In this study we will investigate the differences between these models for the vortex flow.

The term that remains to be modeled in the Reynolds stress transport equation (6) is the turbulent transport term. The molecular and turbulent diffusion of the Reynolds stresses, $\mathcal{D}_{ij}$, is

$$\hat{\boldsymbol{e}}_i\hat{\boldsymbol{e}}_j\mathcal{D}_{ij} = \nabla\cdot(\nu\nabla\bar{\bar{\tau}} - \boldsymbol{T}) \tag{14}$$

where $\boldsymbol{T}$ is the turbulent flux of Reynolds stresses. In the present computation we will adopt the Daly and Harlow[19] model that reads

$$\boldsymbol{T} = -c_s(K/\varepsilon)\bar{\bar{\tau}}\cdot\nabla\bar{\bar{\tau}} \tag{15}$$

where $c_s = 0.25$. With the assumptions we have made for the vortex, the diffusion becomes

$$\mathcal{D}_{ij} = \frac{1}{r}\frac{\partial}{\partial r}\left(r\left(\nu + c_s\frac{K}{\varepsilon}\overline{u^2}\right)\frac{\partial\tau_{ij}}{\partial r}\right) + \mathcal{D}_{ij}^{(\mathrm{ex})} \tag{16}$$

where the extra diffusion $\mathcal{D}_{ij}^{(\mathrm{ex})}$ consists of all terms that emanate from the nonzero $\hat{\boldsymbol{\theta}}$ derivatives of the unit vectors. The nonzero components of the extra diffusion read

$$\begin{aligned}\mathcal{D}_{uv}^{(\mathrm{ex})} &= \frac{1}{r}\frac{\partial}{\partial r}\left(c_s\frac{K}{\varepsilon}\overline{uv}(\overline{u^2} - \overline{v^2})\right) \\ &+ c_s\frac{K}{\varepsilon}\frac{\overline{uv}}{r}\left(\frac{\partial}{\partial r}(\overline{u^2} - \overline{v^2}) - 4\frac{\overline{v^2}}{r}\right) - 4\nu\frac{\overline{uv}}{r^2} \\ \mathcal{D}_{uu}^{(\mathrm{ex})} &= -\mathcal{D}_{vv}^{(\mathrm{ex})} = \frac{1}{r}\frac{\partial}{\partial r}\left(-2c_s\frac{K}{\varepsilon}\overline{uv}^2\right) \\ &- 2c_s\frac{K}{\varepsilon}\left(\frac{\overline{uv}}{r}\frac{\partial\overline{uv}}{\partial r} + \frac{\overline{v^2}(\overline{u^2} - \overline{v^2})}{r^2}\right) - 2\nu\frac{\overline{u^2} - \overline{v^2}}{r^2}\end{aligned} \tag{17}$$

Finally, the Daly and Harlow[19] model for the dissipation reads

$$\mathcal{D}^{(\varepsilon)} = \frac{1}{r}\frac{\partial}{\partial r}\left(r\left(\nu + c_\varepsilon\frac{K}{\varepsilon}\overline{u^2}\right)\frac{\partial\varepsilon}{\partial r}\right) \tag{18}$$

where $c_\varepsilon = 0.15$.

B. Algebraic Reynolds Stress Modeling

An alternative of writing the system of equations in terms of the Reynolds stresses is to reformulate the equations in terms of the Reynolds stress anisotropy and the turbulent kinetic energy. In flows where the anisotropy varies slowly in time and space, the transport equation for the Reynolds stress anisotropy tensor reduces to an implicit algebraic relation. Also in many inhomogeneous flows of engineering interest, the flow is steady and the advection and diffusion of the Reynolds stress anisotropy may be neglected.[20,21] This is equivalent to assuming that the advection and diffusion of the individual Reynolds stresses scale with those of the turbulent kinetic energy.

The advection of the Reynolds stress tensor is, however, dependent on the coordinate system and would, thus, lead to an algebraic relation and a model that is dependent on the choice of coordinate system. This could be of major importance in flows with strong streamline curvature, such as strongly rotating flows. In circular flows it is, therefore, most appropriate to neglect the advection of the anisotropy following a streamline, which is similar to neglecting the rate of change of the anisotropy following a fluid particle. For the vortex flow considered in this study, this is fulfilled exactly by including the algebraic terms in Eq. (10). In a more general flow it is possible to define a Galilean invariant curvilinear coordinate system based on the acceleration vector.[10]

By the use of the general linear pressure–strain model in Eq. (12), the transport equation for the Reynolds stress anisotropy tensor reads

$$\begin{aligned}\frac{K}{\varepsilon}\left(\frac{\partial a_{ij}}{\partial t} - \mathcal{D}_{ij}^{(a)}\right) &= -\left(L_1^0 + \frac{L_1^1}{2}\frac{\mathcal{P}}{\varepsilon}\right)a_{ij} + 2L_2\frac{K}{\varepsilon}S_{ij} \\ &+ L_3\frac{K}{\varepsilon}\left(a_{ik}S_{kj} + S_{ik}a_{kj} - \frac{2}{3}a_{kl}S_{lk}\delta_{ij}\right) - L_4\frac{K}{\varepsilon}\left(a_{ik}\Omega_{kj}^* - \Omega_{ik}^*a_{kj}\right)\end{aligned} \tag{19}$$

The advection of the Reynolds stress anisotropy is, for the vortex, exactly included in the modified rotation rate tensor

$$\boldsymbol{\Omega}^* = \boldsymbol{\Omega} - \boldsymbol{\Omega}^{(r)}\,|\,L_4 \tag{20}$$

where $\boldsymbol{\Omega}^{(r)}$ is given by Eq. (11). The L coefficients are related to the C coefficients in Eq. (12) through

$$\begin{aligned}L_1^0 &= C_1^0\,|\,2 - 1, \qquad L_1^1 = C_1^1 + 2, \qquad L_2 = C_2/2 - \tfrac{2}{3} \\ L_3 &= C_3/2 - 1, \qquad L_4 = C_4/2 - 1\end{aligned} \tag{21}$$

The transport equation for the turbulent kinetic energy is obtained by taking half of the trace of the equation for the Reynolds stress tensor

$$\frac{\partial K}{\partial t} - \mathcal{D}^{(K)} = \mathcal{P} - \varepsilon \tag{22}$$

where the diffusion of turbulent kinetic energy is

$$\mathcal{D}^{(K)} = \frac{1}{2}\mathcal{D}_{ii} = \frac{1}{r}\frac{\partial}{\partial r}\left(r\left(\nu + c_s\frac{K}{\varepsilon}\overline{u^2}\right)\frac{\partial K}{\partial r}\right) \tag{23}$$

Neglecting the time dependency and the molecular and turbulent diffusion of the Reynolds stress anisotropy, the left-hand side of Eq. (19), leads to an algebraic relation

$$\begin{aligned}0 &= -\left[L_1^0 + \left(L_1^1\,|\,2\right)(\mathcal{P}/\varepsilon)\right]a_{ij} + 2L_2(K/\varepsilon)S_{ij} + L_3(K/\varepsilon) \\ &\times\left(a_{ik}S_{kj} + S_{ik}a_{kj} - \tfrac{2}{3}a_{kl}S_{lk}\delta_{ij}\right) - L_4(K/\varepsilon)\left(a_{ik}\Omega_{kj}^* - \Omega_{ik}^*a_{kj}\right)\end{aligned} \tag{24}$$

Also in the algebraic equation, advection of the Reynolds stress anisotropy is exactly included through the modified rotation rate tensor $\boldsymbol{\Omega}^*$ [Eq. (20)]. Thus, the importance of the advection may be investigated by excluding the $\boldsymbol{\Omega}$ correction.

C. Explicit Algebraic Reynolds Stress Modeling

Using representation theory, Pope[22] proposed that the implicit relation (24) may be solved so that an explicit relation for the anisotropy is obtained. The scalar nonlinearity in $\mathcal{P}/\varepsilon$, because $\mathcal{P} = -Ka_{ij}S_{ji}$, may be expressed as a cubic polynomial that has an explicit solution.[12,23] That will result in a fully explicit and self-consistent algebraic relation for the Reynolds stress anisotropy tensor that may be written as

$$a_{ij} = \beta_1(K/\varepsilon)S_{ij} + \beta_2(K/\varepsilon)^2\left(S_{ik}S_{kj} - \tfrac{2}{3}II_S\delta_{ij}\right) + \beta_4(K/\varepsilon)^2\left(S_{ik}\Omega^*_{kj} - \Omega^*_{ik}S_{kj}\right) \tag{25}$$

where

$$\beta_1 = -(A_1N/Q), \qquad \beta_2 = 2A_1A_2/Q, \qquad \beta_4 = -(A_1/Q) \tag{26}$$

$$Q = N^2 - 2(K/\varepsilon)^2II_{\Omega^*} - \tfrac{2}{3}A_2^2(K/\varepsilon)^2II_S \tag{27}$$

The invariants $II_S \equiv S_{ik}S_{kj}$ and $II_{\Omega^*} \equiv \Omega^*_{ik}\Omega^*_{kj}$, and $N \equiv A_3 + A_4\mathcal{P}/\varepsilon$. The solution to the cubic equation for $\mathcal{P}/\varepsilon$ or N reads

$$N\begin{cases} = (A_3/3) + (P_1 + \sqrt{P_2})^{\frac{1}{3}} + (P_1 - \sqrt{P_2})^{\frac{1}{3}}, & P_2 \geq 0 \\ = (A_3/3) + 2\left(P_1^2 - P_2\right)^{\frac{1}{6}} \\ \quad \cos\left[\tfrac{1}{3}\arccos\left(P_1\big|\sqrt{P_1^2 - P_2}\right)\right], & P_2 < 0 \end{cases} \tag{28}$$

where

$$P_1 = \left[\frac{A_3^2}{27} + \left(\frac{A_1A_4}{6} - \frac{2}{9}A_2^2\right)\left(\frac{K}{\varepsilon}\right)^2II_S - \frac{2}{3}\left(\frac{K}{\varepsilon}\right)^2II_{\Omega^*}\right]A_3$$

$$P_2 = P_1^2 - \left[\frac{A_3^2}{9} + \left(\frac{A_1A_4}{3} + \frac{2}{9}A_2^2\right)\left(\frac{K}{\varepsilon}\right)^2II_S + \frac{2}{3}\left(\frac{K}{\varepsilon}\right)^2II_{\Omega^*}\right]^3 \tag{29}$$

When computing the third root, one needs to make sure that the real root is returned even for negative arguments, and the arccos function should return an angle between 0 and π. The A coefficients are related to the L coefficients in Eq. (19) through

$$A_1 = 2L_2/L_4, \qquad A_2 = L_3/L_4$$
$$A_3 = -\left(L_1^0\big|\,L_4\right), \qquad A_4 = -\tfrac{1}{2}\left(L_1^1\big|\,L_4\right) \tag{30}$$

Thus, the Reynolds stress anisotropy is fully explicitly expressed in terms of the mean flow gradient and the turbulent timescale (K/ε). This replaces the transport equation for the anisotropy tensor and is used together with the transport equations for the turbulent kinetic energy [Eq. (22)] and the dissipation rate [Eq. (9)]. The Reynolds stresses are directly related to the anisotropy through definition (13). The Daly and Harlow[19] modeling of the transport of K and ε [Eqs. (23) and (18)] is also kept at this level of modeling.

The formal reduction of the full Reynolds stress transport model results in a two-equation turbulence model where the standard eddy-viscosity assumption is replaced with a more complete constitutive relation. This can be compared to the eddy-viscosity assumption that relates the Reynolds stresses linearly to the mean flow strain rate tensor:

$$a_{ij} = -2C_\mu(K/\varepsilon)S_{ij} \tag{31}$$

where the coefficient $C_\mu = 0.09$. Even the first term in Eq. (25) gives a much better description of the anisotropy because the effective $C_\mu^{\text{eff}} = -\beta_1/2$ is not a constant but is dependent on the local flow state. Moreover, the eddy-viscosity assumption does not give realistic values of the normal Reynolds stress components, and thus, the Daly and Harlow[19] diffusion model could not be used. The diffusion terms in the K and ε equations, for the standard eddy-viscosity K–ε model, are thus modeled using a simple gradient diffusion model that reads

$$\mathcal{D}^{(K)} = \frac{1}{r}\frac{\partial}{\partial r}\left(r\left(\nu + \frac{C_\mu}{\sigma_K}\frac{K^2}{\varepsilon}\right)\frac{\partial K}{\partial r}\right)$$
$$\mathcal{D}^{(\varepsilon)} = \frac{1}{r}\frac{\partial}{\partial r}\left(r\left(\nu + \frac{C_\mu}{\sigma_\varepsilon}\frac{K^2}{\varepsilon}\right)\frac{\partial \varepsilon}{\partial r}\right) \tag{32}$$

where the standard values $\sigma_K = 1.0$ and $\sigma_\varepsilon = 1.3$ are used.

III. Numerical Methods and Boundary Conditions

The system of equations is integrated in time using a first-order implicit method (backward Euler) from a prescribed initial condition. For every time step, the system of equations is iterated until convergence by reducing the residual 6 decades. Second-order central differences on a staggered grid is used for the spatial discretization.

Typically, 1000 time steps for two-equation computations and 2000 time steps for full Reynolds stress computations were used in the computations. Decreasing the time step did not influence the result. Here, 100 computational points in the radial direction were used, 20 points with an equidistant distribution within $r = 2R_c$ and the other points smoothly stretched toward the outer boundary. Doubling the number of grid points alters the computed circulation by less than 1%.

To keep the symmetry for the velocity components in the cylindrical coordinate system, the tangential velocity as well as the Reynolds shear stress component must be zero. Moreover, the normal Reynolds stress components as well as K and ε should have zero spatial derivatives. The boundary conditions at $r = 0$ are

$$V = \frac{\partial\overline{u^2}}{\partial r} = \frac{\partial\overline{v^2}}{\partial r} = \frac{\partial\overline{w^2}}{\partial r} = \frac{\partial K}{\partial r} = \frac{\partial \varepsilon}{\partial r} = \overline{uv} = 0 \tag{33}$$

The outer edge of the computational domain is situated far away from the vortex. The boundary condition for the tangential velocity is obtained by assuming that the flow is inviscid, and thus, the vortex circulation Γ approaches a constant. The boundary condition for the turbulence quantities are set in such a way that an initial freestream turbulence level would properly decay in time. This requires, however, that the computational domain is large enough so that the production and the diffusion at the outer boundary, $R_{\max}$, are negligible. In this study $R_{\max} \approx 100$ core radii. The boundary conditions at $r = R_{\max}$ are

$$\frac{\partial}{\partial r}(rV) = \frac{\partial\overline{u^2}}{\partial r} = \frac{\partial\overline{v^2}}{\partial r} = \frac{\partial\overline{w^2}}{\partial r} = \frac{\partial K}{\partial r} = \frac{\partial \varepsilon}{\partial r} = \frac{\partial\overline{uv}}{\partial r} = 0 \tag{34}$$

The system of equations and the boundary conditions are specified in a differential form using the symbolic manipulation tool MAPLE. FORTRAN subroutines that compute the discrete system matrix are then automatically generated with the aid of routines written in MAPLE. The sources of programming errors are then reduced to the much more limited number of lines of the MAPLE code compared to the final FORTRAN code.

IV. Test Case and Computational Results

In the test case adopted for this study we will eliminate all effects of ambient influence, such as atmospheric turbulence, stratification, or the other vortex, to study the isolated effect of vortex decay subjected to self-generated turbulence. The outer edge boundary condition is, thus, put far away, and the vortex is initiated assuming that it extends to infinity. LIDAR measurements of an aircraft trailing vortex at the Memphis airport, case 1252,[24,25] will be used for a qualitative comparison with the computations. The case is characterized by low ambient turbulence during nighttime and slow vortex decay rate. Despite the low turbulence levels, it is still believed that the ambient conditions are of importance for the vortex decay rate. Comparisons with the observed vortex decay rate are, thus, not fully relevant because these effects are not present in the computations. Nevertheless, the measured circulation profiles at $t = 5$ s will be used as initial conditions for the computations, and the computational results will be compared to profiles measured at $t = 55$ s, shown in Figs. 1 and 2.

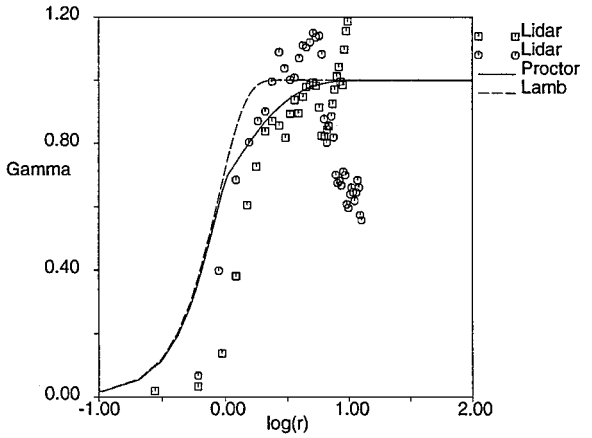

Fig. 1 Different initial circulation profiles [Proctor[1] and Lamb (see Ref. 26)] compared to measured profiles at $t = 5$ s.

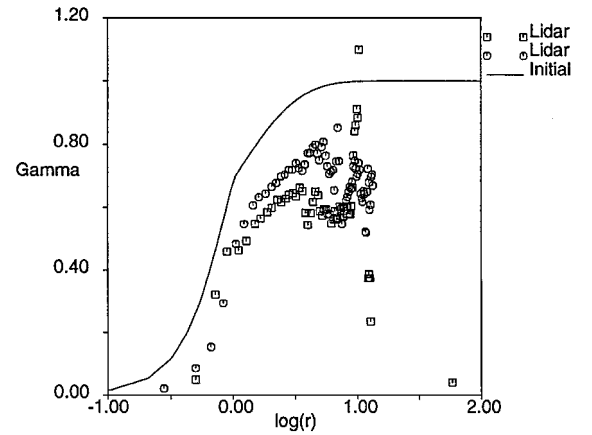

Fig. 2 Measured circulation profiles at $t = 55$ s compared to the initial profile.[1]

A. Initial Conditions

The vortex circulation, defined as $\Gamma \equiv 2\pi r V$, increases from zero at the core center and levels up to a fairly constant level, Γ_0, outside of the vortex core. The vortex strength Γ_0 is typically around 350 m^2/s and the core radius R_c, defined as the position of the peak tangential velocity, is typically around 1.8 m. That gives a Reynolds number based on Γ_0 of about 20×10^6.

The problem is made nondimensional based on $\Gamma_0 = 350\,m^2/s$ and $R_c = 1.8$ m. That means that all lengths are normalized by R_c, time by R_c^2/Γ_0, velocity by Γ_0/R_c, turbulent kinetic energy and Reynolds stresses by Γ_0^2/R_c^2, and dissipation rate by Γ_0^3/R_c^4.

Laminar vortices where the viscosity is constant are self-similar in time with the normalized vortex circulation given by

$$\Gamma = 1 - \exp[-\alpha r^2] \tag{35}$$

This is referred to as a Lamb vortex (Ref. 26, p. 253). The coefficient α is usually around 1.26, which gives a maximal normalized velocity $V_{max} \approx 0.11$.

Measurements of aircraft wing-tip trailing vortices over airfields show that the typical circulation distribution is somewhat different from a Lamb vortex. By considering a large set of data from vortex measurements, Proctor[1] proposed an alternative form that better matches the data:

$$\Gamma = \begin{cases} 1.4\left(1 - \exp\left[-10(1/B)^{\frac{3}{4}}\right]\right)(1 - \exp[-1.2527r^2]), & r < 1 \\ 1 - \exp\left[-10(r/B)^{\frac{3}{4}}\right], & r \geq 1 \end{cases} \tag{36}$$

where B is the (normalized) span width of the airplane that generates the vortex. This gives the normalized maximal velocity $V_{max} \approx 0.11$. The initial circulation profiles [Lamb (see Ref. 26) and Proctor[1]] are compared to measured data in Fig. 1. The vortex is initially prescribed according to Eq. (36) using the normalized span width $B = 17.7$. The initial profile does not perfectly match the data, but the initial core radius was fit to a large number of measurements and the data in Fig. 1 are only one set of measurements.

The initialization of the turbulence is, however, not obvious because turbulence field measurements within the vortex are rare. The measured atmospheric turbulence could, however, act as a lower limit for the initial vortex turbulence. For the low turbulence case considered (Dallas 1997 Wake Vortex Data Set CD-ROM, personal communication with Proctor, Flight Dynamics and Control Division, NASA Langley Research Center), the turbulent kinetic energy $K \sim 0.02\,m^2/s^2$ and the dissipation rate $\varepsilon \sim 10^{-5}\,m^2/s^3$. That corresponds to a normalized turbulence level of the order of $K \sim 10^{-7}$ and $\varepsilon \sim 10^{-12}$. The integral length scale is of the order of 10^2 (core radius), which may be unrealistically high for the self-generated turbulence in the vortex. The dissipation rate is, however, universal over all turbulent scales, and by assuming a length scale of the vortex self-generated turbulence in the order of unity, one obtains $K \sim 10^{-8}$ and $\varepsilon \sim 10^{-12}$. At these low initial levels the growth rate is so slow that the flow remains nearly laminar in the RANS computations.

The rollup of a wing-tip vortex takes place in the very near-wake region, and a fully developed and nearly symmetric vortex is formed within the near wake. In the experiment by Chow et al.,[4] rollup happened within less than one chord length from the trailing edge of the wing, whereas Devenport et al.[5] observed a much more extended rollup of the near wake. The vortex is fully turbulent, although the turbulence shear stress in the core is strongly suppressed. The turbulence level at the most downstream measured section is of the order of 10% of the axial freestream velocity, and the maximum swirl velocity was of the same order as the axial freestream velocity. By assuming that the turbulence length scale is of the order of the core radius, one obtains the normalized $K = 10^{-4}$ and $\varepsilon = 10^{-6}$. Using that as initial condition, one found that the turbulence levels quickly decrease to some asymptotic level that is about one order of magnitude lower, shown in Fig. 3a. During that process, the high-intensity turbulence diffuses the tangential velocity before the decay rate settles down to some asymptotic level. The transient behavior of the circulation is seen in Fig. 4a. By the setting of the initial turbulence level to the order of that asymptotic state, the initial transient is eliminated, and the computed time history becomes somewhat independent of small initial variations and the exact form of the initial profiles.

The turbulence is initially assumed homogeneous, or uniform, with the normalized $K_0 = 10^{-5}$ and $\varepsilon_0 = 10^{-8}$, which gives a freestream turbulence level of 2% of V_{max} and the turbulent macrolength scale $\Lambda = K^{3/2}/\varepsilon \approx 3.2$. In the differential Reynolds stress computations, the normal Reynolds stress anisotropy is prescribed to be zero, and the normalized Reynolds stress shear component $\overline{uv} = K_0 V(r)$. Figure 4b shows a typical time evolution of a computation initiated with these conditions.

The vortex flow was integrated for a time period of 50 s, which corresponds to 600 vortex turnover times defined as R_c/V_{max}. The computed results may then be compared to the measured data at $t = 55$ s. Sarpkaya and Daly[2] introduced an alternative timescale based on the downsweep of the vortex pair and the initial vortex separation $t^* = V_0 t/B$, where $V_0 = \Gamma_0/(2\pi B)$. Note that 55 s corresponds to $t^* = 3.0$.

B. Reynolds Stress Transport Models

The flow in the core of the vortex approaches solid body rotation, and thus, the production of the turbulence is suppressed. In the outer part of the vortex, the flow gradually changes from rotation dominated to completely strain dominated. It is well known that standard eddy-viscosity two-equation models, such as the K–ε model, are unable to describe the turbulence in rotation-dominated flows satisfactorily. Also the response of different RST models are known to be substantially different in rotation-dominated flows.

The results using the different RST models are shown in Fig. 5. The SSG model is known to perform better than the LRR model in rotation-dominated flows, and the results show that the linear SSG compares well with the measurements in this case whereas the LRR model predicts a decay rate slower than observed. Moreover,

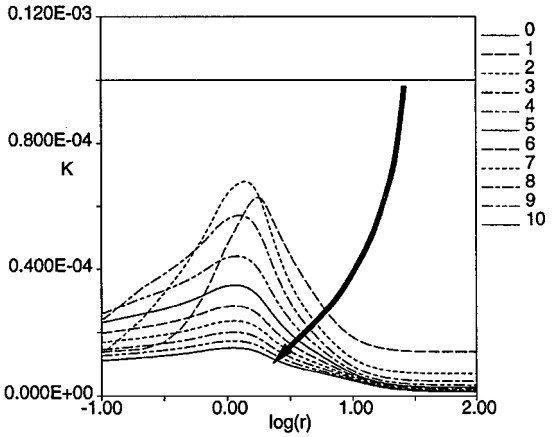

a) High levels, $K = 10^{-4}$ and $\varepsilon = 10^{-6}$

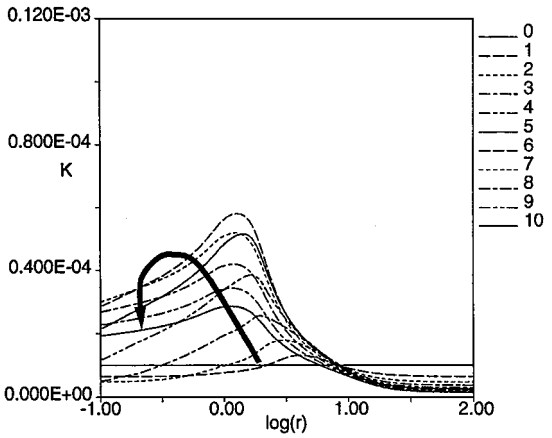

b) Nominal levels, $K = 10^{-5}$ and $\varepsilon = 10^{-8}$

Fig. 3 Evolution of the computed turbulent kinetic energy subjected to different initial turbulent levels using EARSM based on SSG. (Spacing between each line is 5 s.)

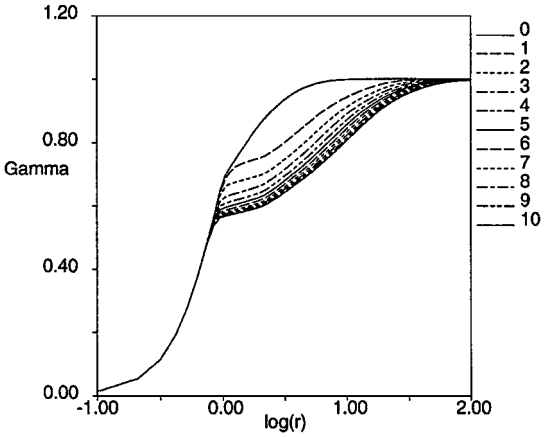

a) High levels, $K = 10^{-4}$ and $\varepsilon = 10^{-6}$

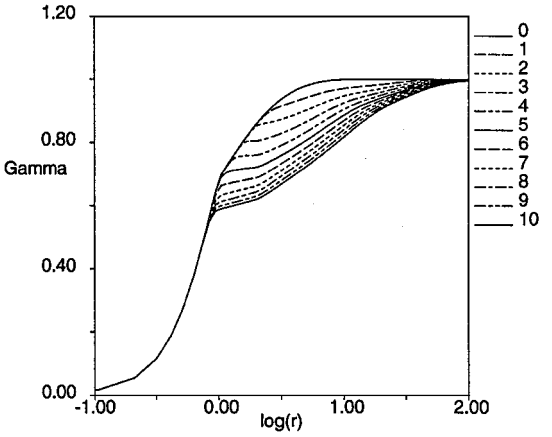

b) Nominal levels, $K = 10^{-5}$ and $\varepsilon = 10^{-8}$

Fig. 4 Evolution of the computed circulation subjected to different initial turbulent levels using EARSM based on SSG. (Spacing between each line is 5 s.)

no overshoot in circulation could be seen, which is in line with observations. A further discussion about a possible overshoot is given in Sec. IV.E.

Figure 5 also shows the Reynolds shear stress for the different RST models. The models correctly predict the strong damping of the turbulence in the vortex core, but in the outer part of the vortex the two models predict very different turbulence shear stresses. The low $\overline{uv}$ values predicted using LRR are consistent with the slow vortex decay rate. Figure 6 shows the turbulent kinetic energy, which, opposite to $\overline{uv}$, do not approach zero in the vortex core. This has also been observed by Devenport et al.[5] experimentally and was explained as influence from the surrounding turbulence.

C. Algebraic Reynolds Stress Models

Reynolds stress transport models are still not widely used in engineering methods, and so an interesting question is, is it possible to obtain computational results similar to the full SSG by means of much simpler two-equation models?

Self-consistent EARSMs are the most consistent approximations of the basic RST models at a two-equation level. In Fig. 7, computational results using EARSM based on both the linearized SSG and the LRR are shown. The EARSM level of modeling follows the behavior of the full Reynolds stress models they are based on. The EARSM based on the LRR predicts a low decay rate of the vortex whereas the EARSM based on the linearized SSG predicts a vortex decay rate in line with observations. For comparison, the result from using the standard K–ε eddy-viscosity model is also shown in Fig. 7. As expected, the vortex decay rate is very much overpredicted, and there is a massive overshoot in the circulation profile.

An important difference between the differential and algebraic form of the linearized SSG is the prediction of the Reynolds shear stress and the turbulent kinetic energy (Fig. 6). In the outer parts of the vortex the EARSM predicts a much lower $\overline{uv}$ compared to the full RST. However, this has just a small implication on the mean swirl velocity as long as the shear stress in and near the vortex core is reasonably predicted.

In the EARSM computations, the weak equilibrium assumption is made in a Galilean invariant curvilinear coordinate system. The importance of that is investigated by computing one case, EARSM based on SSG, where the weak equilibrium assumption is made in an inertial system. That is equivalent to letting $\boldsymbol{\Omega}^* = \boldsymbol{\Omega}$ in Eq. (24). The results are labeled "SSG no rot" in Fig. 7 and show a vortex decay rate that is completely in error. This result demonstrates the importance of the correct treatment of the advection term in algebraic modeling of turbulent strongly curved flows. Neglecting this effect makes EARSM as bad as standard eddy-viscosity models.

The EARSM approach taken for this study is that the explicit solution is fully self-consistent. That means that the implicit algebraic relation is exactly solved without further assumptions. The importance of this approach is assessed by computing the case using the EARSM based on the linearized SSG model, but without considering the solution for $\mathcal{P}/\varepsilon$ or N in Eq. (28), but rather to use the equilibrium value in homogeneous shear. This is similar to the Gatski and Speziale model,[13] but in this study we do not consider the regularization of the denominator to avoid singular behavior that is a part of the Gatski and Speziale model, and thus, the only difference between the models is the consistency condition. This model is labeled "G&S" in Fig. 8. The G&S model gives a similar vortex decay rate compared to the SSG, but the circulation profile is distorted just outside of the core, and the decay rate is somewhat lower in the outermost regions of the core. It is, however, possible that the regularization would cure this behavior, but that is not considered in this study.

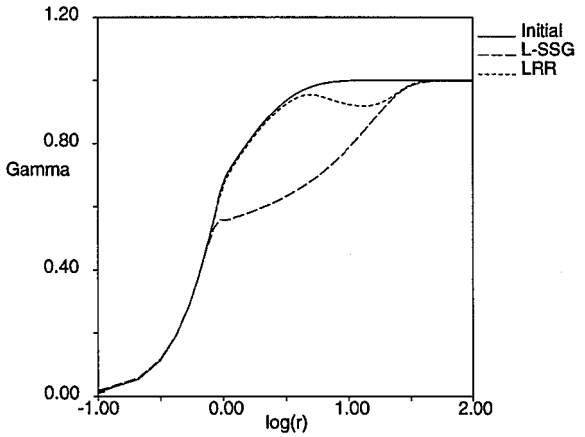

Computed vortex circulation

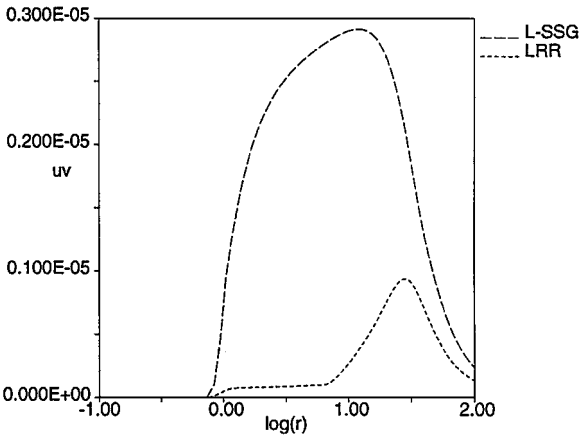

Shear stress

Fig. 5 Profiles at $t = 55$ s using different RST models; flow initiated using the Proctor[1] profile.

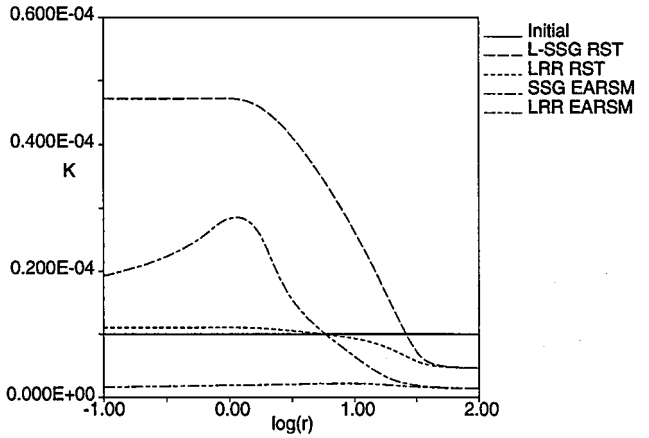

Fig. 6 Computed turbulent kinetic energy profiles at $t = 55$ s using different models; flow initiated using the Proctor[1] profile.

The turbulent diffusions of K and ε in the EARSM computations are determined using the Daly and Harlow model, which relates the diffusivity to the u fluctuations [Eqs. (23) and (18)]. The importance of the diffusion modeling is determined by using the standard eddy-viscosity gradient diffusion model of the diffusion Eq. (32) as a comparison. To obtain somewhat realistic values on the diffusivity, the C_μ coefficient is not taken as a constant but is related to β_1 in Eq. (26), $C_\mu = -\beta_1/2$. Figure 8 shows this comparison for the EARSM based on the linearized SSG model, where "SSG" and "SSG nut" label the computations using the Daly and Harlow,[19] and eddy-viscosity modeling of the diffusion, respectively. There are only minor differences between the two modeling approaches indicating that the turbulent diffusion modeling is not a critical issue.

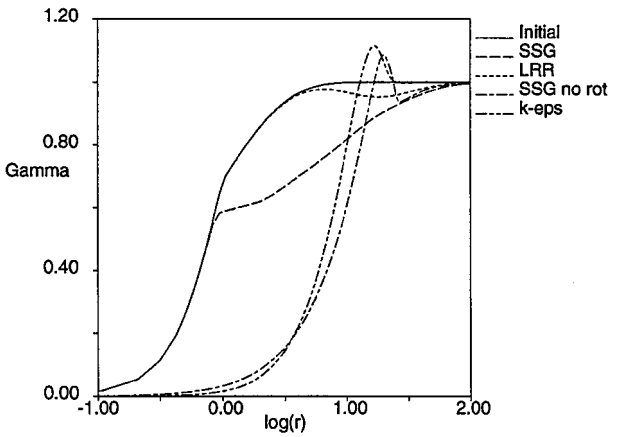

Computed vortex circulation

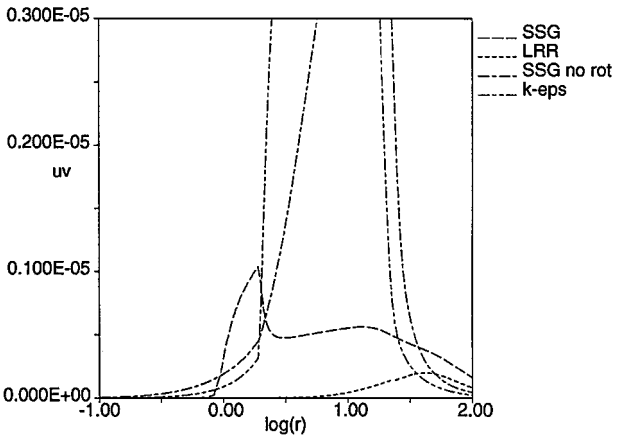

Shear stress

Fig. 7 Profiles at $t = 55$ s using different EARSMs and the standard eddy-viscosity K–ε model (k-eps); flow initiated using the Proctor profile.[1]

The LRR and SSG models gave very different behavior for this flow, and one important difference between the two models is the C_2 coefficient before the S_{ij} term in Eq. (12). In the linearized SSG model, the equilibrium value $C_2 = 0.36$ is used, whereas $C_2 = 0.8$ in the LRR model, which corresponds to rapid distortion theory. The algebraic form of the LRR model (using the newly recalibrated coefficients) is especially attractive because the complexity of the algebra in three-dimensional mean flows is very reduced.[14,23] It is possible to keep exactly the same algebraic form by changing the L coefficients in Eq. (21) so that the A coefficients in Eq. (30) remain unchanged and the C_2 coefficient takes the value of 0.36 rather than 0.8. That leads to the alternative set of C coefficients where $C_1^0 = 4.92$, $C_1^1 = 1.65$, $C_2 = 0.36$, $C_3 = 2$, and $C_4 = 0.378$. Because the A coefficients remain unchanged compared to the LRR model, the basic EARSM remains unchanged, and the simple algebraic form is preserved. The only difference enters through the modified rotation rate tensor to account for the advection. The computational result from using this model, "mix" in Fig. 8, is much closer to the SSG model than the LRR model. Thus, it is reasonable to believe that this mechanism is the most important difference between the SSG and LRR models for this flow and that the decay rate of the vortex is much controlled by the C_2 coefficient. This mixed model is, however, not yet another proposal of a linear pressure–strain model, but only constructed to assess the differences between the SSG and LRR models and the importance of the C_2 coefficient.

D. Variation of the Initial Circulation Profile

The observations in the preceding sections are made using an initial circulation profile that corresponds to observed trailing vortices. That initial circulation profile deviates somewhat from the Lamb vortex (see Ref. 26) that has been used in previous studies of trailing vortices (for example, see Ref. 7). The two different initial profiles

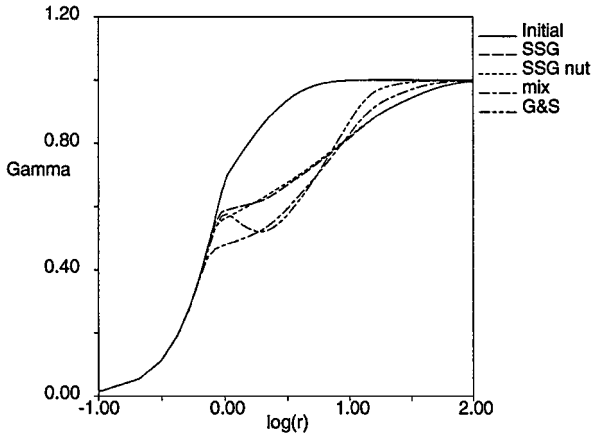

Computed vortex circulation

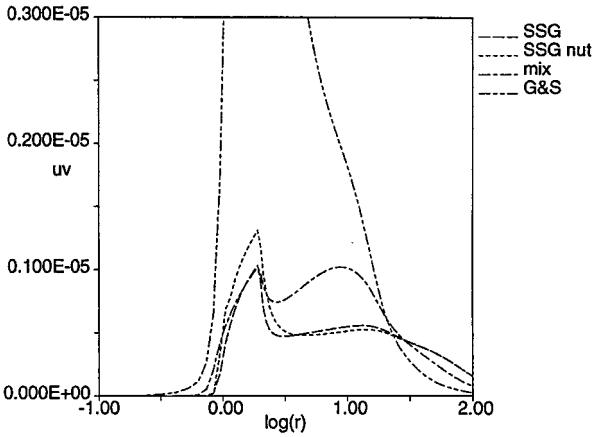

Shear stress

Fig. 8 Profiles at $t = 55$ s using different EARSMs based on the linearized SSG model; flow initiated using the Proctor profile.[1]

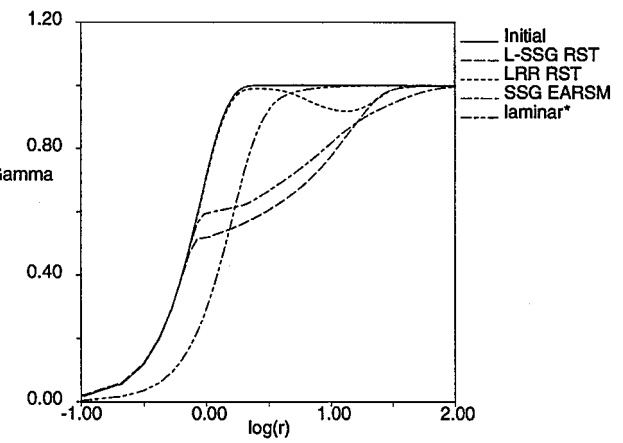

Fig. 9 Computed vortex circulation profiles at $t = 55$ s using different models; laminar results were obtained at $Re = 10^4$; flow initiated using the Lamb profile (Ref. 26).

are shown in Fig. 1. The computations with this alternative (Lamb) initial profile follows the previous computations (Fig. 9). The SSG-based models, in differential form as well as in algebraic form, give reasonable results whereas the LRR-based models strongly underpredict the vortex decay rate. Also here one may observe that the algebraic modeling assumption gives results comparable to the full RST models.

Also shown in Fig. 9 are the laminar results where the Reynolds number has been decreased from 20×10^6 to 10^4; otherwise there would have been almost no difference between the initial and final profiles. The laminar result shows a completely different nature where the vortex decays mostly from the core and outward giving an increased vortex radius while leaving the exterior part of the vortex unaffected. The laminar decay rate is also much slower than the turbulent decay rate.

E. Comments on the Obtained Results

There are some questions concerning the obtained results that need to be further discussed. The vortices studied here are linearly stable according to Rayleigh's[27] stability criterion.

The model computations show an initial growth of turbulence that saturates and starts to decrease slowly (Fig. 3b). The level at which the turbulence saturates is, however, fairly low, $K \sim 10^{-5}$ (normalized by Γ_0 and R_c). This could be compared to the large-eddy simulations by Ragab and Sreedhar,[6] where the computations were interrupted when $K \sim 10^{-4}$, or the measurements by Devenport et al.,[5] where the maximal level at the final streamwise position was $K \sim 10^{-4}$.

If the initial turbulence level in the model computations is prescribed much higher than the saturation level, no initial growth could be seen. The turbulence rapidly decreases to about the saturation level (Fig. 3a). If the initial turbulence level is prescribed to be very low, the initial growth is very weak, but still positive, and the saturation level will not be reached within the time period investigated here.

The same principal behavior could be observed using models based on SSG, as well as LRR, but the saturation level is much lower when using the LRR model.

The question is if this behavior, predicted by the models, is physically reasonable or not. We know that the vortex is linearly stable (at least if we ignore that the mean flow is not stationary), and thus, we do not have exponential growth of any of the eigenmodes. Also if the eigenmodes are orthogonal, we would expect an overall exponential decay of any disturbances. However, the eigenmodes are not orthogonal, and thus, there exists a mechanism for disturbances to grow. The perhaps most classical example of this is plane Couette flow that is linearly stable for all Reynolds numbers[28] but transient growth nevertheless could lead to turbulence.

Schmid et al.[29] studied the eigenvalue sensitivity for the Batchelor vortex, for example, which is linearly unstable due to an axial velocity deficit. Large sensitivity is closely connected to the possibility of transient growth. For this case they found strong transient growth that was not related to the most unstable mode but rather due to large sensitivities of stable or weakly unstable modes. From this, it is not unrealistic to expect similar behavior for other types of vortices, even if they are linearly stable, and that an alternative growth mechanism may exist.

To our knowledge it is not clear whether the Lamb type of vortex could sustain turbulence or not. Numerical experiments (for example, large-eddy simulation by Ragab and Sreedhar[6]) did not show any evidence of sustained turbulence for the linearly stable case. However, the saturated turbulence level could be quite low without any large structures, which is typical for cases with a highly unstable mode, and may be overlooked if not explicitly searched for. These computations were interrupted when $K \sim 10^{-4}$, which is one order of magnitude larger than the saturated level predicted by our SSG model computations. Moreover, the stable case computed by Ragab and Sreedhar shows an initial behavior that could be interpreted as transient growth.

An other question concerns a possible overshoot in the circulation profile. The angular momentum must be conserved, and Govindaraju and Saffman[11] showed that a vortex that entrains the ambient at a rate greater than that due to molecular diffusion must develop a circulation overshoot. However, no overshoot could be seen in our computational results, except for the strongly diffusive eddy-viscosity K–ε model. In the analysis by Govindaraju and Saffman, the Reynolds shear stress $\overline{uv}$ was assumed to decrease with increasing radius at a rate faster than r^{-2}. That means that an effective eddy viscosity must decrease with increasing radius. In our computations, we have initiated the turbulence with a uniform K and ε field, which gives an effective eddy viscosity that far exceeds the molecular viscosity also at the outer boundary of the computational domain. The angular momentum or circulation

will, thus, be transported out of the computational domain without developing any overshoot of circulation within the domain.

The assumption of an initially uniform turbulent field is not unreasonable when studying vortices in atmospheric conditions because the atmospheric turbulence level may act as a lower limit on the eddy viscosity at increasing radius. This could actually be the reason for the lack of experimentally observed circulation overshoots.

V. Conclusions

The turbulent vortex flow investigated is strongly affected by rotation, and even at the Reynolds stress transport modeling level, there are important differences between different models. All models based on the Reynolds stress transport equations, differential as well as algebraic, predict the strong suppression of the turbulence within the vortex core, consistent with observations. However, models based on the LRR pressure–strain model predict that the turbulence is almost completely suppressed also in the exterior part of the vortex, and the predicted vortex decay rate is much lower than observed. In that sense, models based on SSG perform more in line with observations. Computations show a fully turbulent vortex outside of the stabilized vortex core, and the vortex decay rate is of the same order as observed decay rates during low turbulent ambient conditions. The computations were made by assuming a vortex that extends to infinity, and thus, any real influence from ambient conditions are not included. The comparison with measured data is, therefore, not fully relevant because strong correlations between ambient conditions and vortex decay rates has been observed and direct comparisons should be avoided. For the idealized case of an isolated vortex, it is not obvious which of the SSG or LRR models give the most physically reasonable results, nor if the isolated vortex is capable of sustaining turbulence at all. However, the particular observation used in this study was one of the slowest decaying ones, and thus, it would be somewhat surprising if the idealized case would substantially deviate from the observed one.

EARSMs are attractive due to reduced complexity and computational effort compared to full RST models. The computational results using EARSM closely follow the results obtained with the full RST models. It is, however, important that the algebraic assumption is made in a streamline-based coordinate system. Neglecting this effect makes the model as bad as the eddy-viscosity $K-\varepsilon$ model, which strongly overpredicts the vortex decay rate. Moreover, it is important that the EARSM is based on a self-consistent approach where the implicit algebraic relation is exactly solved without further assumptions. The modeling of the diffusion terms in the $K-\varepsilon$ equations is not very important in this flow. The anisotropy diffusivity approach by Daly and Harlow[19] gives results comparable to the standard eddy-diffusivity approach as long as the eddy diffusivity is based on an effective C_μ determined from the EARSM relations rather than a universal constant (usually 0.09).

Acknowledgments

The authors gratefully acknowledge funding for this study from the Aeronautical Research Institute of Sweden (FFA) and from the Flight Dynamics and Control Division at NASA Langley Research Center. This study was performed at the Institute for Computer Applications in Science and Engineering, NASA Langley Research Center, during a visit by the first author. The authors would like to thank F. Proctor for introducing us to this problem and sharing with us his experience in this field.

References

[1]Proctor, F. H., "The NASA-Langley Wake Vortex Modelling Effort in Support of an Operational Aircraft Spacing System," AIAA Paper 98-0589, Jan. 1998.

[2]Sarpkaya, T., and Daly, J. J., "Effect of Ambient Turbulence on Trailing Vortices," *Journal of Aircraft*, Vol. 24, No. 6, 1987, pp. 399–404.

[3]Sarpkaya, T., "Decay of Wake Vortices of Large Aircraft," *AIAA Journal*, Vol. 36, No. 9, 1998, pp. 1671–1679.

[4]Chow, J. S., Zilliac, G. G., and Bradshaw, P., "Mean and Turbulence Measurements in the Near Field of a Wingtip Vortex," *AIAA Journal*, Vol. 35, No. 10, 1997, pp. 1561–1567.

[5]Devenport, W. J., Rife, M. C., Liapis, S. I., and Follin, G. J., "The Structure and Development of a Wing-Tip Vortex," *Journal of Fluid Mechanics*, Vol. 312, 1996, pp. 67–106.

[6]Ragab, S., and Sreedhar, M., "Numerical Simulation of Vortices with Axial Velocity Deficits," *Physics of Fluids*, Vol. 7, No. 3, 1995, pp. 549–558.

[7]Zeman, O., "The Persistence of Trailing Vortices: A Modeling Study," *Physics of Fluids*, Vol. 7, No. 1, 1994, pp. 135–143.

[8]Speziale, C. G., Sarkar, S., and Gatski, T. B., "Modeling the Pressure–Strain Correlation of Turbulence: An Invariant Dynamical Systems Approach," *Journal of Fluid Mechanics*, Vol. 227, 1991, pp. 245–272.

[9]Launder, B. E., Reece, G. J., and Rodi, W., "Progress in the Development of a Reynolds-Stress Turbulence Closure," *Journal of Fluid Mechanics*, Vol. 41, 1975, pp. 537–566.

[10]Girimaji, S. S., "A Galilean Invariant Explicit Algebraic Reynolds Stress Model for Turbulent Curved Flows," *Physics of Fluids*, Vol. 9, No. 4, 1997, pp. 1067–1077.

[11]Govindaraju, S. P., and Saffman, P. G., "Flow in a Turbulent Trailing Vortex," *Physics of Fluids*, Vol. 14, No. 10, 1971, pp. 2074–2080.

[12]Girimaji, S. S., "Fully Explicit and Self-Consistent Algebraic Reynolds Stress Model," *Theoretical and Computational Fluid Dynamics*, Vol. 8, No. 6, 1996, pp. 387–402.

[13]Gatski, T. B., and Speziale, C. G., "On Explicit Algebraic Stress Models for Complex Turbulent Flows," *Journal of Fluid Mechanics*, Vol. 254, 1993, pp. 59–78.

[14]Taulbee, D. B., "An Improved Algebraic Reynolds Stress Model and Corresponding Nonlinear Stress Model," *Physics of Fluids A*, Vol. 4, No. 11, 1992, pp. 2555–2561.

[15]Lumley, J. L., "Computational Modeling of Turbulent Flows," *Advances in Applied Mechanics*, Vol. 18, Academic, New York, 1978, pp. 123–176.

[16]Shabbir, A., and Shih, T. H., "Critical Assessment of Reynolds Stress Turbulence Models Using Homogeneous Flows," NASA TM 105954, ICOMP-92-24, CMOTT-92-12, 1992.

[17]Wallin, S., and Johansson, A. V., "A New Explicit Algebraic Reynolds Stress Turbulence Model Including an Improved Near-Wall Treatment," *Proceedings Flow Modeling and Turbulence Measurements VI*, edited by C.-J. Chen, C. Shih, J. Lienau, and R. J. Kung, Balkema, Rotterdam, The Netherlands, 1996, pp. 399–406.

[18]Wallin, S., and Johansson, A. V., "An Explicit Algebraic Reynolds Stress Model for Incompressible and Compressible Turbulent Flows," *Journal of Fluid Mechanics* (to be published); also Aeronautical Research Inst. of Sweden (FFA), TN 1997-51, Bromma, Sweden, 1997.

[19]Daly, B. J., and Harlow, F. H., "Transport Equations in Turbulence," *Phys. Fluids*, Vol. 13, No. 11, 1970, pp. 2634–2649.

[20]Rodi, W., "The Prediction of Free Turbulent Boundary Layers by Use of a Two-Equation Model of Turbulence," Ph.D. Dissertation, Dept. of Mechanical Engineering, HTS/72/24, Imperial College of Science and Technology, London, 1972.

[21]Rodi, W., "A New Algebraic Relation for Calculating the Reynolds Stresses," *Zeitschrift für Angewandte Mathematik und Mechanik*, Vol. 56, No. 3, 1976, pp. T219–221.

[22]Pope, S. B., "A More General Effective-Viscosity Hypothesis," *Journal of Fluid Mechanics*, Vol. 72, 1975, pp. 331–340.

[23]Johansson, A. V., and Wallin, S., "A New Explicit Algebraic Reynolds Stress Model," *Proceedings of the Sixth European Turbulence Conference*, edited by S. Gavrilakis, L. Machiels, and P. A. Monkewitz, Kluwer, 1996, pp. 31–34.

[24]Campbell, S. D., Dasey, T. J., Freehart, R. E., Heinrichs, R. M., Matthews, M. P., and Perras, G. H., "Wake Vortex Field Measurement Program at Memphis," AIAA Paper 96-0399, Jan. 1996.

[25]Campbell, S. D., Dasey, T. J., Freehart, R. E., Heinrichs, R. M., Matthews, M. P., Perras, G. H., and Rowe, G. S., "Wake Vortex Field Measurement Program at Memphis," TN Data Guide, Project Report NASA/L-2, Jan. 1997.

[26]Saffman, P. G., *Vortex Dynamics*, Cambridge Univ. Press, New York, 1992.

[27]Rayleigh, Lord, "On the Dynamics of Revolving Fluids," *Proceedings of the Royal Society of London, Series A: Mathematical and Physical Sciences*, Vol. 93, 1916, pp. 148–154.

[28]Herron, I. H., "Observations on the Role of Vorticity in the Stability Theory of Wall Bounded Flows," *Studies in Applied Mathematics*, Vol. 85, No. 3, 1991, pp. 269–286.

[29]Schmid, P. J., Henningson, D. S., Khorrami, M. R., and Mujeeb, R. M., "A Study of Eigenvalue Sensitivity for Hydrodynamic Stability Operators," *Theoretical and Computational Fluid Dynamics*, Vol. 4, No. 5, 1993, pp. 227–240.

J. P. Gore
Associate Editor